



Laser-induced surface-tension-driven flows in liquids

Jon P. Longtin^{a,*}, Kunio Hijikata^b, Kuniyasu Ogawa^b

^a Department of Mechanical Engineering, State University of New York at Stony Brook, Stony Brook, NY 11794–2300, U.S.A.

^b Department of Mechano-Aerospace Engineering, Tokyo Institute of Technology, 2-12-1 Oh-okayama, Meguro-ku, Tokyo 152, Japan

Received 8 October 1997; in final form 3 April 1998

Abstract

High-intensity, short-pulse laser radiation incident on the free surface of an absorbing dielectric liquid results in heating that can alter the liquid surface tension, causing Marangoni convection. This flow can dominate the transport of thermal energy in the liquid. In this work, both a scaling analysis and a full numerical simulation of the governing equations are performed. A thermal mechanism is proposed as the driving force for these flows. The dependence on beam size and temperature increase in the liquid is investigated, with good agreement found among the scaling analysis, numerical simulations and experimental data obtained from a previous study. The importance of natural convection and thermal conduction on the fluid-thermal transport was assessed numerically, with both found to be negligible for this liquid–laser system. Velocity and temperature profiles at the liquid surface are also discussed. © 1998 Elsevier Science Ltd. All rights reserved.

Nomenclature

a radius of heated region [m]
 C_p specific heat [$\text{J kg}^{-1} \text{K}^{-1}$]
 E_0 pulse energy [J]
 g gravitational acceleration, $g = 9.82 \text{ m s}^{-2}$
 h liquid height [m]
 k thermal conductivity [$\text{W m}^{-1} \text{K}^{-1}$]
 n time step index
 P pressure [N m^{-2}]
 R radius of liquid container [m]
 r radial coordinate [m]
 T temperature [K]
 ΔT temperature rise in laser-heated region [K]
 t time [s]
 Δt time step in numerical solution [s]
 u velocity [m s^{-1}]
 z axial coordinate from liquid surface [m].

Greek symbols

α absorption coefficient [m^{-1}]
 β coefficient of thermal expansion, $\beta = -1/\rho (d\rho/dT)$ [K^{-1}]

Γ thermal diffusivity [$\text{m}^2 \text{s}^{-1}$]
 γ dummy variable
 δ momentum diffusion depth, $\delta = (\nu t)^{1/2}$ [m]
 δ_t radiation penetration depth, $\delta_t = \alpha^{-1}$ [m]
 μ dynamic viscosity [$\text{N s}^{-1} \text{m}^{-2}$]
 ν kinematic viscosity [$\text{m}^2 \text{s}^{-1}$]
 ρ density [kg m^{-3}]
 σ surface tension [N m^{-1}]
 τ surface shear [N m^{-2}]
 ζ laser beam edge parameter [m].

Subscripts

ed edge
p laser pulse
 r radial direction
 z axial direction
0 initial
 ∞ ambient.

1. Introduction

Laser-induced surface-tension-driven (LISTD) flows using short-pulse, high-power (SPHP) lasers represent an important and growing class of engineering problems. Application areas include diagnostics, measurement,

* Corresponding author. Fax: 001 516 632 8544; e-mail: jlongtin@ccmail.sunysb.edu

bioengineering, droplet vaporization and combustion, and microcircuit repair. Research involving LISTD flows is particularly timely due to the rapid progress being made in contemporary laser technology, which is providing more powerful and reliable lasers at a larger number of wavelengths and at reduced costs.

Research involving SPHP laser interactions with a liquid surface, however, is scarce. Da Costa and Escalona [1] and Da Costa [2] have investigated the flow and surface deformation associated with laser heating of absorbing oils, however their work used continuous-wave (CW) lasers, and the time scale of the heating was in the order of 0.1 s. Bennett et al. have recently demonstrated a laser-based surface texturing process for magnetic disk substrates that relies in part on surface-tension effects [3, 4]. Their liquids were molten metals at high temperatures. Hijikata et al. [5] performed several novel experimental measurements using SPHP laser interacting with organic liquids: kerosene, ethanol, octane and R113. They proposed an ionization-based concentration model to explain the LISTD fluid motion.

Recently the authors presented experimental results for LISTD flows using a short-pulse laser interacting with a strongly absorbing dielectric liquid [6]. A XeCl excimer laser with a wavelength of 308 nm was used to irradiate the free surface of ethanol with a small amount of photochromic dye added for absorption and flow visualization. The irradiated liquid turned red, generating a circular spot, initially the radius of the laser beam, that subsequently expanded due to LISTD flow, as shown in Fig. 1. The radius of the expanding dye spot versus time was measured and reported for several incident intensities and laser beam diameters.

This paper presents both a simple engineering expression and a full numerical simulation of LISTD flows. The work focuses on typical liquids, which are dielectric and in the liquid state at room temperature. Examples include alcohols, refrigerants, fuels and water. The purposes of the work are to demonstrate that a thermal mechanism is responsible for LISTD flows, pro-

vide a detailed analysis of the fluid flow and thermal transport, determine the governing parameters, and assess the importance of buoyancy and thermal conduction in these flows.

The simple engineering expression for LISTD flows is developed from a scaling analysis of the governing equations. For the numerical simulations, the SIMPLEC technique [7, 8] is used to model the two-dimensional, axisymmetric flow and thermal transport in the liquid. The time-dependent expansion of the laser-heated liquid region is computed from both the scaling analysis and the numerical solution, and compared to prior experimental data by the authors [6], with good agreement found. The numerical simulation also provides velocity and temperature information at the liquid surface and interior.

2. Formulation

When a laser pulse strikes the free surface of an absorbing liquid, the temperature T of the liquid at and near the surface increases due to absorption of the laser pulse. This temperature increase results in a change (usually a decrease) in the liquid surface tension σ , which in turn imparts a shear stress τ at the liquid surface, giving rise to fluid motion and thermal transport (Fig. 1). Buoyancy effects in the heated liquid may also contribute to the fluid flow. For a circular, axisymmetric laser beam incident on a quiescent liquid surface, a temperature gradient will arise in the radial direction only. The surface shear, which arises due to the radial temperature gradient, $\partial T/\partial r$, is coupled to the surface velocity gradient (for a Newtonian fluid) as follows:

$$\tau = \frac{\partial \sigma}{\partial r} = \frac{\partial \sigma}{\partial T} \frac{\partial T}{\partial r} = \mu \left. \frac{\partial u_r}{\partial z} \right|_{z=0} \quad (1)$$

Here u_r is the radial velocity. In this work the change in surface tension with temperature, $\partial \sigma/\partial T$, is assumed constant.

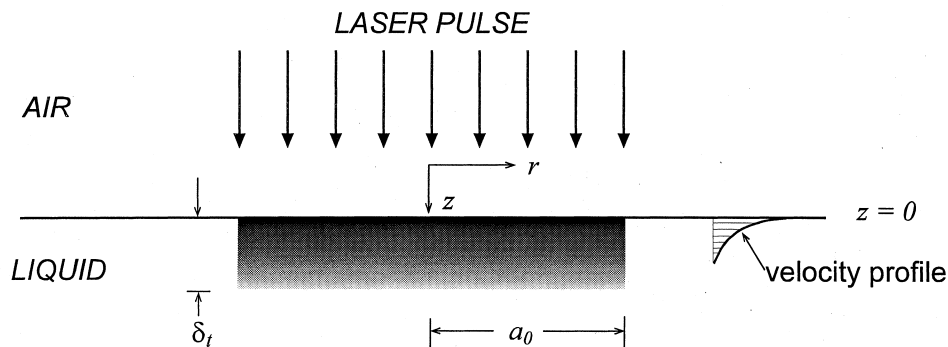


Fig. 1. LISTD heating and flow.

2.1. Governing equations and boundary conditions

The geometry and liquid system for this study are identical to that used in the experimental investigations by Longtin and Hijikata [6]: pure ethanol with a small amount of photochromic (color changing) dye resides in an uncovered circular Petri dish with a radius R of 4.3 cm and liquid height h of 1.2 cm. A XeCl excimer laser pulse with a pulse duration of ~ 25 ns and a wavelength of 308 nm impinges upon the surface, resulting in LISTD flow as shown in Fig. 1. The plane $z = 0$ corresponds to the liquid surface, while $r = 0$ represents the radial centerline of the system. In the experiment, a circular aperture a few cm above the liquid surface is used to generate an axisymmetric, uniform beam spot on the liquid surface with radius a_0 . As such, only a radial temperature gradient is generated at the liquid surface. Thermophysical properties are assumed constant, except for the temperature-dependent surface tension described above and the liquid density, which is used in the Boussinesq approximation for the buoyancy term [9].

The conservation of mass equation is [10]

$$\frac{\partial u_r}{\partial r} + \frac{u_r}{r} + \frac{\partial u_z}{\partial z} = 0. \tag{2}$$

The time-dependent conservation of momentum equations in the radial, r , and axial, z , directions are, respectively:

$$\begin{aligned} \frac{\partial u_r}{\partial t} + u_r \frac{\partial u_r}{\partial r} + u_z \frac{\partial u_r}{\partial z} \\ = -\frac{1}{\rho} \frac{\partial P}{\partial r} + \nu \left(\frac{\partial^2 u_r}{\partial r^2} + \frac{1}{r} \frac{\partial u_r}{\partial r} - \frac{u_r}{r^2} + \frac{\partial^2 u_r}{\partial z^2} \right) \end{aligned} \tag{3}$$

$$\begin{aligned} \frac{\partial u_z}{\partial t} + u_r \frac{\partial u_z}{\partial r} + u_z \frac{\partial u_z}{\partial z} = -\frac{1}{\rho} \frac{\partial P}{\partial z} \\ + \nu \left(\frac{\partial^2 u_z}{\partial r^2} + \frac{1}{r} \frac{\partial u_z}{\partial r} + \frac{\partial^2 u_z}{\partial z^2} \right) + g\beta(T - T_\infty). \end{aligned} \tag{4}$$

The conservation of thermal energy takes the form

$$\frac{\partial T}{\partial t} + u_r \frac{\partial T}{\partial r} + u_z \frac{\partial T}{\partial z} = \Gamma \left(\frac{\partial^2 T}{\partial r^2} + \frac{1}{r} \frac{\partial T}{\partial r} + \frac{\partial^2 T}{\partial z^2} \right). \tag{5}$$

The complete boundary conditions for equations (2)–(5) are:

$$\frac{\partial u_r}{\partial z} = \frac{1}{\mu} \frac{\partial \sigma}{\partial T} \frac{\partial T}{\partial r} \quad \text{at } z = 0 \quad (\text{liquid surface}) \tag{1}$$

$$u_r = 0 \quad \text{at } r = 0, r = R \quad \text{and } z = h \tag{6a}$$

$$u_z = 0 \quad \text{at } z = 0, z = h \quad \text{and } r = R \tag{6b}$$

$$\partial u_z / \partial r = 0 \quad \text{at } r = 0 \tag{6c}$$

$$u_r = u_z = 0 \quad \text{at } t = 0 \tag{6d}$$

$$\partial T / \partial z = 0 \quad \text{at } z = 0 \quad \text{and } z = h \quad (\text{insulated}) \tag{6e}$$

$$\partial T / \partial r = 0 \quad \text{at } r = 0 \quad \text{and } r = R \quad (\text{insulated}) \tag{6f}$$

$$T = T_p(r, z) \quad \text{at } t = 0. \tag{6g}$$

The function $T_p(r, z)$ represents the initial temperature increase in the liquid as a result of heating by the incident laser pulse, as discussed in the next section.

Several assumptions made in the formulation deserve mention. The first is that the interface remains flat during LISTD flow. In practice, small deformations will likely form on the liquid surface as the laser-heated liquid region expands. Similar phenomena have been investigated in the analysis of concentration-induced surface-tension-driven flows, e.g., due to surfactants or contamination on a liquid surface [11, 12]. These effects are neglected in this analysis because the height of the deformations is small compared to the liquid height, and the change in the surface tension in this analysis is relatively small, compared to, e.g., the case when a foreign substance is added to the liquid surface. Additionally, the extremely rapid laser heating will result in rapid expansion of the liquid, which will also deform the surface somewhat, though this effect is neglected. For very thin liquid films, however, surface deformation and rapid expansion effects may have to be accounted for to model the flow accurately.

Second, mass transfer at the interface due to the elevated temperature of the laser-heated liquid is neglected. Since the maximum temperature increase in the experiments was on the order of 10 K, evaporation effects are assumed small. Also, the incident laser light is assumed not to be influenced by vapor from evaporation above the liquid surface. An important transition occurs, however, in LISTD flows when the temperature in the liquid becomes comparable to the boiling point. As observed during the experiments when temperatures above the boiling point were generated in the ethanol, e.g., for highly focused beams, violent ejection of liquid from the surface occurred, causing fluid motion radically different than that observed at lower intensities.

Finally, any deformation of the liquid surface due to the radiation pressure of the intense laser pulse is ignored [13], because the beam arrives at the liquid surface at near-normal incidence and is of a very short duration. Self-focusing of the incident beam due to surface deformations is also ignored due to the extremely short pulse duration (~ 25 ns) of the incident beam [14].

2.2. Temperature distribution in liquid

A liquid must exhibit at least moderate absorption at the laser wavelength for LISTD flow to occur, as liquid heating occurs through the process of absorbing the incident laser pulse. Since the incident pulse duration is so short (~ 25 ns), heating occurs much faster than the conduction and convection time scales in the system, and an initial temperature profile is used at the start of the solution in equation (6g) rather than incorporating a

time-dependent heating term in the energy equation, equation (5).

If the liquid absorbs classically, i.e., the intensity decreases exponentially with distance from the surface, the temperature profile will depend only on the liquid absorption coefficient α and the energy distribution in the laser beam cross section [6, 15]. At very high laser intensities, liquids can exhibit intensity-dependent absorption that can deviate significantly from the classical absorption model [16, 17]. In fact, at high enough incident intensities, even normally transparent liquids can absorb enough laser pulse energy to generate LISTD flows. Longtin and Hijikata characterized the ethanol/dye mixture, and found it to absorb classically for the laser intensities considered in their work [6], thus the temperature is assumed to decrease exponentially with distance z into the liquid.

For the temperature variation within the cross section of the beam, it is noted that excimer lasers have fairly uniform intensity distributions, and the beam was further apertured to allow only the center, most uniform portion of the beam to strike the liquid. The temperature distribution in the azimuthal and radial direction at all parts of the beam except the edge is thus approximated as uniform.

Diffraction after the beam is apertured results in a complicated, interference-dominated intensity near the edge of the heated region. The distance from the aperture to the liquid was kept as small as possible to minimize these edge effects [18]. In the numerical simulation, the edge effects are approximated by a smooth transition in the beam intensity pattern near the edge of the beam, i.e., $r \sim a$, which serves as a compromise between a physically unrealistic step discontinuity and the true, complicated intensity distribution at the liquid surface. The temperature increase in the liquid just after the pulse passes is then

$$\Delta T_p(r, z) = \frac{\Delta T_0 \exp(-\alpha z)}{1 + \exp\left(\frac{r-a}{\zeta}\right)} \quad (7)$$

and $T_p(r, z) = \Delta T_p(r, z) + T_\infty$ in equation (6g), where ΔT_0 is the maximum temperature rise in the liquid and T_∞ is the ambient fluid temperature.

Note that the temperature decays exponentially with distance z into the liquid. The exponential term in the denominator of equation (7) accounts for the transition from the uniform intensity near the center of the beam to zero at distances $r \gg a$. Here ζ is a small number, e.g., ~ 0.01 . The results showed a negligible sensitivity to variations in ζ . The maximum temperature increase occurs at the liquid surface with magnitude:

$$\Delta T_0 = \frac{\alpha E_0}{\pi a_0^2 \rho C_p} \quad (8)$$

In the experiment, the surface temperature was not

measured directly; rather the absorption coefficient α and pulse energy E_0 were measured, and equations (7) and (8) were used to determine the temperature in the liquid [6].

2.3. Scaling and dimensional analysis

To determine the functional dependence on the problem parameters and develop simple engineering criteria to determine when surface-tension-induced flows are important, a dimensional analysis is used to develop a simple model for the surface motion from the governing equations. Referring to Fig. 1, the characteristic scale in the radial direction is initially the width of the heated region, a , thus $r \sim a$, and the heated region radius is initially the laser beam radius: $a = a_0$ at $t = 0$. The radial velocity u_r scales with the surface velocity U , yet to be determined. The characteristic temperature in the system is the temperature difference ΔT between the heated liquid and the ambient.

Surface tension gradients impart a shear force to the liquid surface, causing fluid flow. The surface motion results in momentum diffusion into the liquid, similar to Stokes's first problem of a suddenly accelerated flat plate in an infinite liquid [10]. Accordingly, the characteristic momentum diffusion thickness in the z -direction, δ , scales as $(\nu t)^{1/2}$. The following scaling relations thus result:

$$\frac{\partial u_r}{\partial z} \sim \frac{U}{\delta} = \frac{U}{(\nu t)^{1/2}}; \quad \frac{\partial T}{\partial r} \sim \frac{\Delta T}{a} \quad (9)$$

Here U is the characteristic surface velocity. Inserting these scaling relations into the shear force balance on the surface, equation (1),

$$\frac{U}{\delta} \sim \gamma \frac{\Delta T}{a} \quad (10)$$

where $\gamma = -1/\mu(d\sigma/dT)$, and is a constant.

Initially, the circular region of liquid of radius a_0 very near the liquid surface has its temperature increased by ΔT_0 due to absorption of the laser pulse. The additional thermal energy added to this region is $\propto \Delta T_0 a_0^2$. The radius a of this heated region then increases with time due to the radial surface velocity: $a \sim a_0 + Ut$. As this thin circular portion of the liquid surface radially expands, however, additional, cooler liquid from below comes to the surface, mixes with the original liquid, and reduces the surface temperature. Ignoring conduction, which is negligible at short times ($t < \sim 1$ s) for dielectric liquids [18] the total thermal energy in this thin laser-heated liquid region near the surface remains constant to first order, and is proportional to the product of the temperature increase ΔT and radius of the heated surface region, a . Then the relation between the initial spot size and temperature and the spot size and temperature at time t scales as

$$\Delta T \sim \frac{a_0^2 \Delta T_0}{a^2} \sim \frac{a_0^2 \Delta T_0}{(a_0 + Ut)^2} \quad (11)$$

where ΔT is the temperature increase of the heated liquid at time t .

Inserting equation (11) and the expressions for a and δ , equation (10) becomes, after rearranging,

$$U(a_0 + Ut)^3 \sim \gamma a_0^2 \Delta T_0 (vt)^{1/2}. \quad (12)$$

Equation (12) is a fourth-order polynomial in U . Though this polynomial can be solved numerically, it can be simplified considerably by ignoring a_0 with respect to Ut , i.e., after the spot size has expanded to twice its original radius. Multiplying both sides by t , and solving for $a = Ut$,

$$a(t) \sim (\gamma v^{1/2} a_0^2 \Delta T_0)^{1/4} t^{3/8}. \quad (13)$$

The difference between the exact solution to equation (12) and the approximation in equation (13) has been shown to be small [19]. Further substituting equation (8) for ΔT_0 and the definition for γ into the above,

$$a(t) \sim \left(\frac{-\alpha E_0}{\pi \mu^{1/2} \rho^{3/2} C_p} \frac{d\sigma}{dT} \right)^{1/4} t^{3/8}. \quad (14)$$

When using equation (14), the initial condition $a(0) \sim a_0$ is used. Observe that there is no dependence on the initial spot size, a_0 , except for the initial condition on $a(t)$. The time-dependent temperature can be obtained by inserting equation (14) into equation (11).

2.4. Numerical solution of GDEs

The SIMPLEC algorithm by Van Doormaal and Raithby [8], which is a modified version of Patankar’s SIMPLE algorithm [7], is employed for the numerical solution of equations (1)–(6). A non-uniform, stretched grid is used in both the r - and z -directions because of the potentially large difference in the length scales in the system, e.g., the size of the laser beam versus the diameter of the liquid container, or the absorption depth in the liquid versus the liquid thickness. This allowed more cells to be concentrated near the liquid surface and the laser-heated region. Typical grid sizes were 40 cells in both the r - and z -directions, and the grid scaling was adjusted so that the cell aspect ratio did not exceed about two. A time step Δt of 2×10^{-4} s was used for all calculations. Grid sensitivity studies were conducted to verify that the selected grid adequately captured the essential fluid-thermal behavior of the system. For example, increasing the grid density from 40×40 to 80×80 cells resulted in a difference of less than 3% in the final results. It should be noted that no adjustable parameters are used in the model. Only the liquid thermo-physical properties, beam geometry, and temperature increase in the liquid are required.

For debugging and validation, the code was used to solve a suite of approximately twenty test cases with

known solutions, including uniform flow ($\mu = 0$), Poiseuille flow, Couette flow, pure conduction ($u = v = 0$), and pure convection ($k = 0$). All test cases were run in both the r - and z -directions.

The experiments by Longtin et al. [6] provide the radius of the laser heated liquid region as a function of time. To obtain this information from the numerical simulation, the edge of the heated region is tracked at each time step:

$$a_{cd}^{n+1} = a_{cd}^n + u_{cd} \Delta t \quad (15)$$

where n is an integer, a_{cd}^n is the radius of the dye spot at time $t = n\Delta t$ and u_{cd} is the surface velocity at the radial position a_{cd}^n , which is obtained by linearly interpolating the surface velocity at the two nearest neighboring points. By definition, the initial heated region size is simply the radius of the laser heating beam: $a_{cd}^0 = a_0$.

3. Results and discussion

3.1. Qualitative comparison of scaling analysis with previous experiments

Hijikata et al. [5] performed a series of laser–liquid interaction measurements for ethanol, kerosene, octane and refrigerant R113 by adding a small amount of highly absorbing photochromic (color changing) dye to the liquid, irradiating the free surface with an excimer laser ($\lambda = 308$ nm), and observing the subsequent fluid motion. The liquid was found to spread radially from the irradiation site. Hijikata et al. proposed that the liquid exposed to the incident laser pulse was ionized, and that the surface tension of this ionized liquid was altered due to the presence of charged liquid molecules, giving rise to LISTD flow. A thermal mechanism was not considered.

Unfortunately, the absorption coefficient, required in equation (14) for the scaling analysis, was not reported in their results. They did, however, demonstrate experimentally that the functional dependence of the spot size, a , versus time, t , took the following form for all of the liquids they tested:

$$a \sim t^{0.38}. \quad (16)$$

This functional dependence compares extremely well with that obtained from the scaling analysis in equation (14), where $a \sim t^{0.375}$.

Furthermore, a feature of Hijikata et al.’s data captured by the thermal model that is not explained from their concentration-based model is the deviation in the experimental data for ethanol. The rate of spot-size expansion for ethanol was observed by Hijikata et al. to be slower than the other fluids used in their experiment, though they did not conclusively explain why. This is explained within the context of a thermal model by noting that the volumetric specific heat, ρC_p , for ethanol is about a factor of two greater than that of kerosene, octane and

R113, resulting in a temperature increase only one half that in the other liquids, all else remaining the same, which results in a smaller surface shear force, and hence a slower spot size expansion from equation (14).

3.2. Scaling and numerical results for ethanol

Both the scaling and numerical simulation results discussed in the preceding sections are compared with recent experimental data for the expanding dye spot for ethanol reported by Longtin et al. [6], in which the experiment measured the dye spot expansion as a function of time. The thermophysical parameters used for the modeling are taken from the literature [20, 21], and are shown in Table 1. In all cases, the liquid was contained in a circular glass container with radius of 4.3 cm and a liquid height of 1.2 cm. The liquid had a measured absorption coefficient of 28 cm^{-1} .

In Fig. 2 the dye radius versus time is shown from the experiment, the scaling analysis (equation (14)), and the numerical model for a surface temperature increase of 1.0 K and a heating beam radius of $\sim 0.75 \text{ mm}$. As can be seen, both the scaling and numerical results are in very good agreement with the experimental data up until about $t \approx 0.5 \text{ s}$. Beyond this time, the velocity of the

expanding dye in the experiment decreases below that for the numerical simulations.

One likely reason for the discrepancy between experiment and the model at times greater than $t \approx 0.5 \text{ s}$ is due to small, but unavoidable surface velocity parallel to the liquid surface. These velocities were readily observed several seconds after the laser pulse arrived as the dye spot became severely distorted and moved as a whole across the liquid surface. This surface velocity arises from motion of the air above the liquid surface and slight temperature variations on the liquid surface, e.g., that result from heating by the light source used to illuminate the liquid for the CCD camera, or cooling from evaporation [6]. Though attempts were made to minimize these velocities, such as enclosing the liquid container and using fluorescent light (compared to an incandescent lamp) to minimize radiant heating of the surface, small surface velocities were unavoidable. Typical surface velocities were observed to be in the order of $1\text{--}3 \text{ mm s}^{-1}$.

The measured dye spot expansion velocity computed from the time-dependent spot radius data in Fig. 2 is shown in Fig. 3. The initial dot expansion velocity is very large, but it rapidly decreases with increasing time. This occurs because the thermal energy, initially concentrated in the small laser-irradiated region, is quickly distributed over a much larger area, resulting in a significantly decreased surface temperature. In this example the dye spot expansion velocity becomes comparable to the nominal surface velocity after about 0.4–0.5 s. This time corresponds to the time in Fig. 2 when the spot expansion begins to slow considerably.

In Fig. 4 a larger aperture for the heating beam has been used, resulting in an initial dye spot radius of 5.0 mm, with ΔT_0 remaining at 1.0 K. Again the numerical model captures the dye spot size versus time behavior very well. The scaling analysis overpredicts the observed surface motion by 20–25%, though it still predicts the correct trend and order of magnitude. Note also that the spot size in Fig. 4 after $\sim 1.0 \text{ s}$ is nearly three times that in Fig. 2. This occurs due to the larger aperture used in

Table 1
Thermophysical properties for liquid ethanol

Parameter	Value
ρ (kg m^{-3})	789
μ ($\times 10^{-4} \text{ N s}^{-1} \text{ m}^{-2}$)	10.46
C_p ($\text{J kg}^{-1} \text{ K}^{-1}$)	2456
k ($\text{W m}^{-1} \text{ K}^{-1}$)	0.166
β ($\times 10^{-3}$)	3.0
α (cm^{-1})	28
$d\sigma/dT$ ($\times 10^{-5} \text{ N m}^{-1} \text{ K}^{-1}$)	-8.3

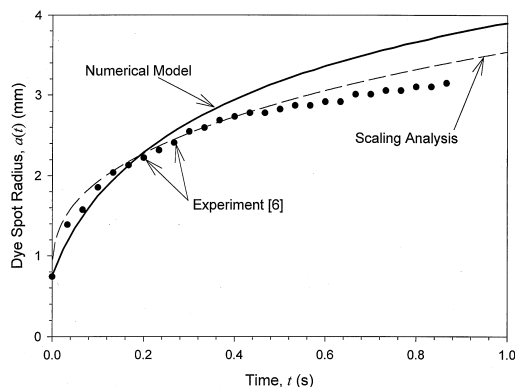


Fig. 2. Model and experiment: $\Delta T_0 = 1.0 \text{ K}$, $a_0 = 0.75 \text{ mm}$.

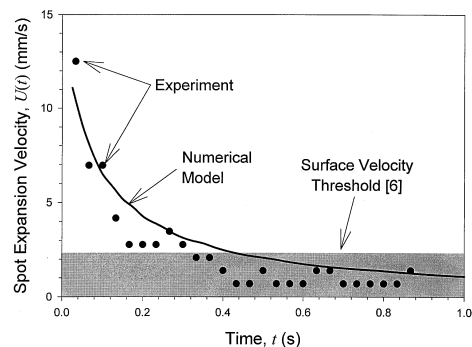


Fig. 3. Dye edge surface velocity: $\Delta T_0 = 1.0 \text{ K}$, $a_0 = 0.75 \text{ mm}$.

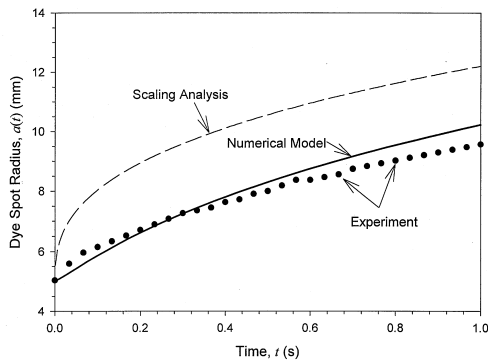


Fig. 4. Model and experiment: $\Delta T_0 = 1.0$ K, $a_0 = 5.0$ mm.

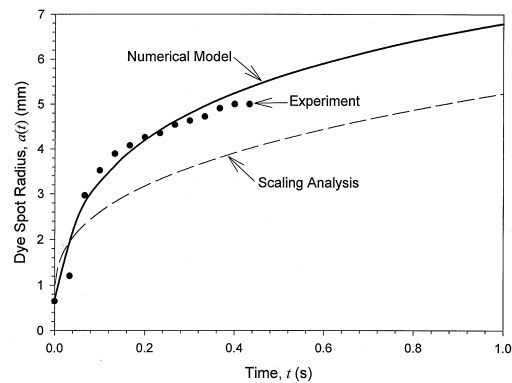


Fig. 6. Model and experiment: $\Delta T_0 = 8.5$ K, $a_0 = 0.68$ mm.

this case, which allows more laser light to pass, and hence more thermal energy to be deposited in the liquid (at the same laser fluence), giving rise to more fluid motion.

Next, the model is compared to data for a larger initial temperature increase in the laser-heated liquid region. A lens was used to increase ΔT_0 to about 8.5 K. In Fig. 5 the aperture radius before the lens results in a beam radius of 1.7 mm at the liquid surface. In this case, the deviation from the numerical model becomes apparent for times greater than 0.35 s, as the dye spot in the experiment has nearly stopped expanding after this time due to a large surface velocity for this particular experimental run. The scaling analysis also accurately captures the dye spot expansion, though the surprisingly good agreement with the experimental results is coincidental. It is interesting to note that the model predictions Figs 4 and 5 both result in comparable dye spot sizes (~ 11 mm) after 1 s, as they both involve the same total incident laser energy, despite having a different initial heating radius, temperature rise, and time-dependent dye spot radius. The scaling analysis underpredicts the spot expansion by 30% or so.

Experiment and model results are shown for focused

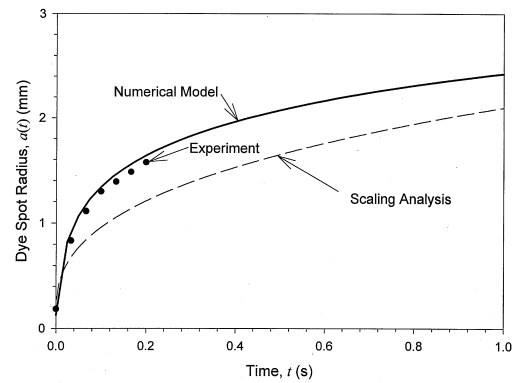


Fig. 7. Model and experiment: $\Delta T_0 = 8.5$ K, $a_0 = 0.125$ mm.

beam cases with a beam radius of 0.68 and 0.125 mm in Figs 6 and 7, respectively. For these cases, the dye spot expansion quickly slowed to the point where the surface velocity was large enough to cause the entire spot to drift; this is the reason the experimental data is reported only for the times shown. The model does a very good job of capturing the dye spot size for these cases, despite a small initial spot size and large temperature increase in the liquid.

3.3. Surface velocity and temperature profiles

In Fig. 8 the surface temperature as a function of r obtained from the model for $a_0 = 0.75$ mm and $\Delta T_0 = 1.0$ K, i.e., the configuration for the results shown in Fig. 2, is shown for times ranging from 25 ms to 1 s. As can be seen, the surface temperature rapidly decreases as the heated region expands, which occurs due to the cylindrical geometry of the heating beam in which the area of the heated liquid region varies as the square of the radius (equation (11)).

Though not shown, results for the surface temperature profile were also computed assuming that thermal con-

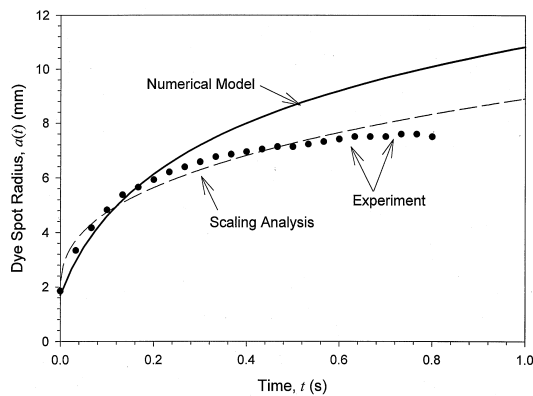


Fig. 5. Model and experiment: $\Delta T_0 = 8.5$ K, $a_0 = 1.4$ mm.

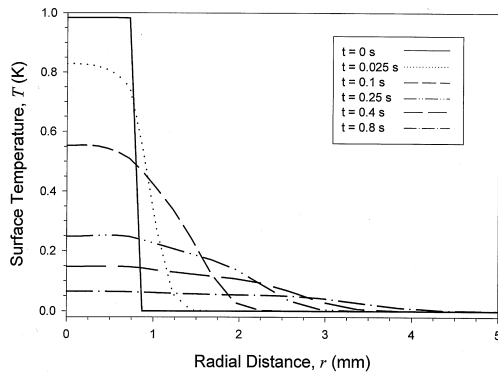


Fig. 8. Surface temperature profiles: $\Delta T_0 = 1.0$ K, $a_0 = 0.75$ mm.

duction was negligible, i.e., $k = 0$, as this assumption was made in the scaling analysis discussed above. In the absence of conduction, the temperature profiles were similar in form to those in Fig. 8, but were about 10% larger at equivalent times. The assumption in the scaling that conduction is negligible is thus reasonable for this liquid–laser system. It should be noted that ethanol, being a dielectric liquid, has a small thermal conductivity ($k = 0.17$ W m⁻¹ K⁻¹); liquids with a larger thermal conductivity, e.g., liquid metals, will have a stronger contribution from conduction in the thermal transport.

The surface velocity as a function of time for the same configuration is shown in Fig. 9. As expected, the velocity is initially confined to the regions in which there is a temperature gradient, which, for a uniform-intensity laser beam, occurs only at the edge of the heated region at $t = 0$. It is illustrative to refer to Fig. 8, as the temperature profiles in that figure correspond to similar times as those for the velocity profiles in Fig. 9. The surface velocity very quickly approaches a peak value, but then rapidly decays as the liquid in the heated region is convected radially outward. This same qualitative behavior is observed in the experimental data in Fig. 3: the velocity is initially large (~ 15 mm s⁻¹ at $t = 25$ ms), but rapidly

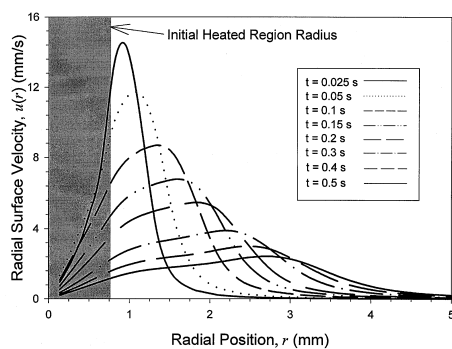


Fig. 9. Surface velocity profiles: $\Delta T_0 = 1.0$ K, $a_0 = 0.75$ mm.

decreases with increasing time as the dye spot size expands. In Fig. 10 the surface velocities are computed for very short times after the laser pulse arrives. Recall that the pulse duration is on the order of nanoseconds, thus the liquid heating is nearly instantaneous. Velocity profiles are shown for times of 1, 2, 4, 8 and 16 ms after the pulse arrives. The nearly instantaneous laser heating coupled with the large temperature gradient near the edge of the dye region results in large surface velocities just after the pulse arrives.

The impact of buoyancy forces on the surface velocity profiles was investigated by performing calculations with and without the buoyancy term in equation (4). Values of the surface velocity change by less than 0.2% for all cases in this work, indicating that, for this laser–liquid system, buoyancy plays a negligible role in the flow. For longer pulse durations and thicker penetration depths into the liquid, however, buoyancy effects may become significant.

4. Conclusions

This work presents results from both a scaling analysis and a numerical simulation of the governing equations for laser-induced surface-tension-driven flow. A thermal mechanism has been proposed as the driving mechanism for the flow. Model results are compared with experimental results from a previous work that investigated XeCl excimer laser pulses interacting with an ethanol–dye solution. Both the scaling and numerical results for the time-dependent expansion of the laser-heated liquid region are in good agreement with the experimental results. Discrepancies at longer times between the model and experiment are attributed to the presence of a small surface velocity that distorted the dye spot radius expansion in the experiment. The importance of natural convection and thermal conduction on the fluid-thermal transport was assessed numerically, with both found to

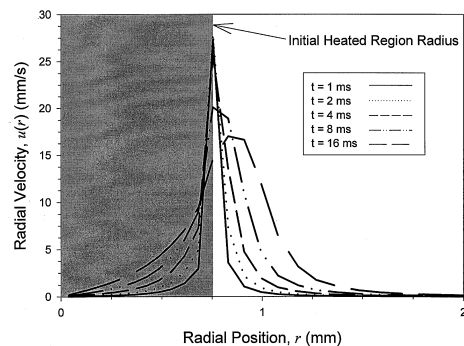


Fig. 10. Surface velocity profiles just after pulse arrival: $\Delta T_0 = 1.0$ K, $a_0 = 0.75$ mm.

be negligible for this liquid–laser system. Velocity and temperature profiles at the liquid surface are also presented, and it is observed that the temperature distribution and surface velocity rapidly decay after the laser pulse arrives.

References

- [1] G. Da Costa, R. Escalona, Time evolution of the caustics of a laser heated liquid film, *Applied Optics* 29 (1990) 1023–1033.
- [2] G. Da Costa, Optical visualization of the velocity distribution in a laser-induced thermocapillary liquid flow, *Applied Optics* 32 (1993) 2143–2151.
- [3] T.D. Bennett, D.J. Krajnovich, C.P. Grigoropoulos, P. Baumgart, A.C. Tam, Marangoni mechanism in pulsed laser texturing of magnetic disk substrates, *Journal of Heat Transfer* 119 (1997) 589–596.
- [4] T.D. Bennett, D.J. Krajnovich, The dynamics of surface melting during laser processing of materials, *Proceedings of the ASME 32nd National Heat Transfer Conference*, vol. 9, HTD-347, New York, 1997. pp. 138–146.
- [5] K. Hijikata, S. Uchida, K. Ogawa, Visualization of free surface phenomena using the photochromic dye activation method. *ASME/JSME Thermal Engineering Conference*, vol. 3, 1995, pp. 439–444.
- [6] J.P. Longtin, K. Hijikata, K. Ogawa, Measurement of pulsed-laser-induced surface-tension-driven flow in liquids, Submitted to the *ASME Journal of Heat Transfer*, 1997.
- [7] S. Patankar, *Numerical Heat Transfer and Fluid Flow*, New York, Hemisphere, 1997, chapters 1–6.
- [8] J.P. Van Doormaal, G.D. Raithby, Enhancements of the SIMPLER method for predicting incompressible fluid flows, *Numerical Heat Transfer* 7 (1984) 147–163.
- [9] A. Bejan, *Convective Heat Transfer*, Wiley, New York, 1984, chapter 4.
- [10] H. Schlichting, *Boundary Layer Theory*, McGraw-Hill, New York, 1979, chapter 3.
- [11] D. Halpern, J.B. Grotberg, Dynamics and transport of a localized soluble surfactant on a thin film, *Journal of Fluid Mechanics* 237 (1992) 1–11.
- [12] O.E. Jensen, J.B. Grotberg, The spreading of heat or soluble surfactant along a thin liquid film, *Physics of Fluids A* 5 (1993) 58–68.
- [13] I.I. Komissarova, G.V. Ostrovskaya, E.N. Shedova, Light pressure-induced deformations of a free liquid surface, *Optics Communications* 66 (1988) 15–20.
- [14] S.A. Viznyuk, S.F. Rastopov, A.T. Sukhodol'skii, On thermocapillary aberrational transformation of laser beams, *Optics Communications* 71 (1989) 239–243.
- [15] M.F. Modest, *Radiative Heat Transfer*, McGraw-Hill, New York, chapter 8.
- [16] J.P. Longtin, C.L. Tien, Efficient laser heating of transparent liquids using multiphoton absorption, *International Journal of Heat and Mass Transfer* 40 (1996) 951–959.
- [17] J.P. Longtin, C.L. Tien, Saturable absorption during high-intensity laser heating of liquids, *Journal of Heat Transfer* 118 (1995) 924–930.
- [18] J.P. Longtin, K. Hijikata, Laser-induced surface tension alteration in liquids, *ASME Proceedings of the 31st National Heat Transfer Conference*, vol. 4, HTD-326, New York, 1996, pp. 63–68.
- [19] J.P. Longtin, K. Hijikata, Laser-induced surface tension flow in ethanol: an experimental investigation, *Proceedings of 1996 Japan–U.S. Seminar on Two-Phase Flow Dynamics*, Fukuoka, Japan, pp. 121–127.
- [20] Chemical Rubber Company (CRC), *CRC Handbook of Chemistry and Physics*, 75th ed., DE Lide (Ed.), CRC Press, Boca Raton, 1995, sections 3, 4, and 6.
- [21] N.B. Vargaftik, *Tables on the Thermophysical Properties of Liquids and Gases*, 1st ed., Wiley, New York, 1975, chapters 4, 13.